Empirical atomic pseudopotentials for AlAs/GaAs superlattices, alloys, and nanostructures

Kurt A. Mäder and Alex Zunger
National Renewable Energy Laboratory, Golden, Colorado 80401
(Received 2 June 1994; revised manuscript received 31 August 1994)

There are numerous instances in semiconductor nanostructure physics where effective-mass approximations are deemed insufficient and "direct diagonalization" approaches that retain the microscopic quasiperiodic potential are needed. In many of these cases there are no free surfaces and charge transfer effects are small, so *fixed, non-self-consistent potential* approaches suffice. To this end we have developed a continuous-space, fully relativistic empirical pseudopotential for AlAs/GaAs, which is carefully fitted to the measured electronic structure of bulk AlAs and GaAs, and to *ab initio* local-density calculations on short- and long-period AlAs/GaAs superlattices. Variations in the anion-cation charge transfer in AlAs and GaAs are simulated by using an As pseudopotential that depends on the number of Al and Ga nearest neighbors. Excellent agreement is demonstrated between the results of the present empirical-pseudopotential method and experiment or *ab initio* calculations for crystal structures exhibiting a variety of local atomic arrangements. The method is suited for large-scale electronic-structure calculations, where a realistic, three-dimensional band structure is important. We illustrate this in the context of plane-wave calculations on (i) 512-atom supercells describing (001) AlAs/GaAs superlattices with rough interfaces, (ii) 2000-atom supercells describing $(AlAs)_n/(GaAs)_m$ superlattices with randomly selected periods (n,m), and (iii) 512-atom AlAs supercells containing clusters of isoelectronic Ga impurities. Our main findings are (i) a transition from an L-like to an X-like conduction-band minimum occurs in the $(AlAs)_1(GaAs)_1$ (001) superlattice as one introduces local interfacial intermixing, (ii) the band-tail states in random superlattices are strongly localized along the growth direction; this is accompanied by a large band-gap reduction, and (iii) while *single* substitutions in AlAs:Ga do not produce bound states, *clusters* of Ga_n within AlAs produce quasibound impuritylike states already for $n = 4$.

I. INTRODUCTION

Most electronic-structure methods currently in use for describing bulk semiconductor systems—ordered compounds, disordered alloys, superlattices with abrupt or rough interfaces, impurities, quantum dots, wells, films, and wires—fall into two general categories: (i) first-principles methods that retain the quasiperiodic microscopic potential $V(\boldsymbol{r})$ in the Hamiltonian $H = -\frac{1}{2}\nabla^2 + V(\boldsymbol{r})$ and determine it self-consistently from the charge density, (ii) methods such as the effective-mass approximation (EMA) and the Kronig-Penney model that replace the array of *microscopic* atomic potentials by rectangular empty boxes separated by walls. Being computationally intensive, class (i) methods are limited to rather small systems (e.g., $\lesssim$100 atoms per computational unit cell), but within this size constraint, arbitrarily complex atomic geometries can be treated (e.g., low-symmetry molecular clusters and supercells, superlattices with interdiffused interfaces, structurally relaxed impurities in solids). Class (ii) methods have the reverse attributes: because the effect of the true microscopic potential is replaced by constant potentials and parabolic bands, only sufficiently *large* systems can be reliably treated. Furthermore, only geometrically simple cases can be handled expediently. For example, superlattices with interdiffused interfaces or three-dimensional random alloys are difficult to describe by such methods. Many physically interesting semiconducting systems—"large systems" with nontrivial geometries—cannot be treated by either type of method. This includes many structurally inhomogeneous quantum structures, such as partially ordered alloys,[1] clustering in alloys,[1] rough interfaces,[2] quantum dots and wires,[3] and nanometer quantum wells.[4] All of these systems require for their description computational unit cells containing $\gtrsim$1000 atoms (so first-principles methods are impractical), yet the geometric complexity and the existence of multiband coupling in the quantum-size limit sometimes preclude the use of simple effective-mass approximations. A possible strategy for this class of problems is offered by the tight-binding (TB) approach.[5–7] This approach retains a microscopic potential $V(\boldsymbol{r})$, but restricts severely both the variational flexibility of the basis set and the range of interaction between atoms. A small number of fictitious atomic orbitals per atom serve as basis functions and interactions are cut off at the second-nearest or third-nearest neighbor. Efficient algorithms, which exploit the localized nature of the basis functions, can be used to solve the tight-binding Hamiltonian. A far more flexible basis set is formed by plane waves. However, the Hamiltonian matrix in this basis is not diagonally dominated or sparse.

Recently,[8] it was shown how $[-\frac{1}{2}\nabla^2 + V(\boldsymbol{r})]\psi_i = \varepsilon_i\psi_i$,

 ©1994 The American Physical Society

with a quasiperiodic potential $V(\boldsymbol{r})$, can be diagonalized directly very efficiently, even for ~1000-atom systems in a highly flexible plane-wave basis set, provided that $V(\boldsymbol{r})$ is a given, fixed potential. Such an approach circumvents the weaknesses of both the EMA and the TB model. Applications require a reliable microscopic potential. Although such potentials are complicated for systems containing free surfaces, it should be possible to find accurate potentials for bulk systems. In the past, $V(\boldsymbol{r})$ was fitted to the observed bulk band structure of zinc blende compounds.[9–11] This is insufficient for nanostructures, because (i) the long wavelength (small momentum $\boldsymbol{q}$) components of $V(\boldsymbol{q})$ needed in nanostructures are undetermined by fitting bulk zinc blende properties. Extrapolation of $V(\boldsymbol{q})$ from zinc blende reciprocal lattice vectors ($|\boldsymbol{q}| \geq \frac{2\pi}{a}\sqrt{3}$, where a is the lattice constant) to smaller $|\boldsymbol{q}|$ values can be inaccurate, so one needs to *explicitly* fit properties of structures with larger repeat unit cells; (ii) fitting the binary compounds AC and BC does not by itself produce a consistent potential for the common atom C needed in calculations for, e.g., AC/BC interfaces; (iii) adjusting a local $V(\boldsymbol{r})$ to produce some given energy levels $\varepsilon_i = \langle\psi_i| -\frac{1}{2}\nabla^2 + V(\boldsymbol{r})|\psi_i\rangle/\langle\psi_i|\psi_i\rangle$ can be accomplished with almost arbitrarily poor wave functions $\psi_i(\boldsymbol{r})$, unless one constrains the latter in some physically meaningful fashion.

In this work, we present an empirical pseudopotential that overcomes the limitations (i)–(iii) noted above: We fit it to the bulk results at a *series* of volumes (thus, a range of $\boldsymbol{q}$'s), as well as to local-density approximation (LDA) results for superlattices (thus, small $\boldsymbol{q}$'s). Furthermore, we make it depend on the local atomic environment, thus simulating charge transfer effects. Finally, we compare the wave functions with LDA-calculated ones.

In the traditional fitting procedure of the empirical-pseudopotential method (EPM),[10] one adjusts the Fourier transform of the potential $V(\boldsymbol{G})$ ("form factors") at a small number of reciprocal lattice vectors $\boldsymbol{G}$ of the zinc blende structure, until the band structure agrees with experimental data. To obtain a more complete knowledge of the potential, a table of form factors at a large number of additional reciprocal lattice vectors [i.e., a *quasicontinuous* function $V(\boldsymbol{q})$] is needed. This was obtained in the past by interpolation,[12,13] or by fitting an algebraic form of the potential to the zinc blende form factors.[14] We can write the crystal potential $V(\boldsymbol{r})$ as a superposition of atomic potentials $v_\alpha(\boldsymbol{r})$, which we assume to be spherically symmetric, i.e.,

$$V(\boldsymbol{r}) = \sum_{n,\alpha} v_\alpha(|\boldsymbol{r} - \boldsymbol{\tau}_\alpha - \boldsymbol{R}_n|)$$

$$= \frac{1}{\Omega_c}\sum_{\alpha}\sum_{\boldsymbol{G}} e^{i\boldsymbol{G}\cdot(\boldsymbol{\tau}_\alpha - \boldsymbol{r})} v_\alpha(|\boldsymbol{G}|), \qquad (1)$$

where the first sum runs over all positions $\boldsymbol{\tau}_\alpha$ within the cell as well as the unit cell vectors $\boldsymbol{R}_n$, while the second reciprocal-space sum runs over all atomic types α and reciprocal lattice vectors $\boldsymbol{G}$, and Ω_c is the unit cell volume. By writing the crystal potential $V(\boldsymbol{r})$ in Eq. (1) as a sum over *fixed*, screened atomic pseudopotentials, we assumed that the atomic potentials do not change much from one system to another ("transferability"). This is not always the case. For example, deep inside the AC region in a AC/BC superlattice, we expect the potential of the C atom to be similar to that in bulk AC and similarly for the C potential deep inside the BC region. At the interface, however, the C atom can have nA and mB nearest neighbors, so neither the C potentials of bulk AC nor that of bulk BC are appropriate. Standard empirical-pseudopotential[12–14] approaches still attempt to describe the AC/BC system using a single, "average" C potential, assuming, therefore, that the charge transfer is environment independent. Assuming a single C potential has an important consequence: the form factors $V(\boldsymbol{G})$ at superlattice reciprocal lattice vectors that are *not* zinc blende reciprocal lattice vectors (NZB), depend on the *difference* of the A and B atomic form factors, but not on the C atom.[13] In fact, one can write $v(\boldsymbol{G}_{\mathrm{NZB}}) = [v_A(\boldsymbol{G}_{\mathrm{NZB}}) - v_B(\boldsymbol{G}_{\mathrm{NZB}})]\, S(\boldsymbol{G}_{\mathrm{NZB}})$, where $S(\boldsymbol{G})$ is a geometrical structure factor. In other words, there is no additional scattering of the valence electrons from the C-atom sublattice in an AC/BC superlattice. In other approaches,[15,16] one assumes that interfaces are infinitely thin, so an electron is either in an AC region or in a BC region, but never at an "interface." In this case, one retains two distinct C potentials (fitted to AC and BC bulk properties, respectively), using each in the corresponding region of the superlattice. Neither approach appears satisfactory. Because the dominant contribution to the screened potential is electrostatic in origin and thus linear in the charge, we can gain insight into the local-environment dependence of the atomic potential by considering the electronic charge. The local charge at atomic sites in III-V semiconductors depends mostly on the *nearest-neighbor* atomic environment.[17] This is true even in transition metal alloys.[18] Thus, assuming efficient screening we can define a C-atom potential that depends on the *number* of nearest-neighbor A and B atoms. For example, in the pseudobinary alloy $A_{1-x}B_xC$, the common ion C can have five distinct nearest-neighbor configurations, viz., the five tetrahedral clusters $A_{4-n}B_n$, where $0 \leq n \leq 4$. The potential of the C atom can depend on n through

$$v_C(A_{4-n}B_nC) = f_n\, v_C(AC) + g_n\, v_C(BC), \qquad (2)$$

where $v_C(AC)$ and $v_C(BC)$ are the C potentials in pure AC and BC, respectively, and f_n and g_n are some weight functions. We will present below a simple model to Eq. (2) that incorporates this local-environment dependence into the C pseudopotential.

To achieve an accurate description of the electronic structure of a large variety of atomic configurations, we fitted the atomic pseudopotentials $v_\alpha(q)$ ($\alpha = A, B, C$), using representation (2) for v_C, to (i) the measured band structures, effective masses, and deformation potentials of the binaries, (ii) the experimental AC/BC valence-band offset between the binaries AC and BC, and (iii) the correct "scattering strength" in various substitutional configurations as reflected by LDA calculated level splittings in short-period $(AC)_n/(BC)_n$ superlat-

tices of various orientations. (iv) We verified that the wave function of bulk and superlattices obtained with our pseudopotentials agree well with those obtained in first-principles LDA calculations. To illustrate the utility of these potentials we have applied them to superlattices with nonabrupt interfaces, disordered superlattices, isoelectronic impurity clusters (Sec. IV), and disordered alloys with short-range order (Ref. 19).

II. FITTING OF THE POTENTIALS

A variety of algebraic forms have been used in the past to fit empirical pseudopotentials.[11,14,20] We have not found an existing form that has sufficient flexibility to fulfill all the requirements (i)–(iv) listed in Sec. I. The algebraic form we propose here has been found in the following way. By choosing the origin in the zinc blende unit cell halfway between the two atoms $\alpha = A$ and $\alpha = C$, Eq. (1) can be written for the zinc blende structure as $V(\boldsymbol{r}) = \frac{1}{\Omega_c}\sum_{\boldsymbol{G}}[\cos(\boldsymbol{G}\cdot\boldsymbol{\tau})\,v_s(G) + i\sin(\boldsymbol{G}\cdot\boldsymbol{\tau})\,v_a(G)]\exp(-i\boldsymbol{G}\cdot\boldsymbol{r})$, where $\boldsymbol{\tau} = \frac{a}{8}(111)$, $v_s(G) = v_A(G) + v_C(G)$, and $v_a(G) = v_A(G) - v_C(G)$ are the symmetric and antisymmetric form factors, respectively, and a is the lattice constant.[10] We have initially adjusted $v_s(G)$ and $v_a(G)$ at a small number of zinc blende reciprocal lattice vectors $\boldsymbol{G}$ to fit band energies and effective masses at different unit cell volumes Ω_c. Because the $\boldsymbol{G}$-vector length scales as $\Omega_c^{-\frac{1}{3}}$, this gave us information about the form factors in the neighborhood of each $\boldsymbol{G}$ vector. The shape of the continuous functions v_s and v_a became thus defined on a much finer mesh, and interpolation was less ambiguous. Moreover, determining $v_s(G)$ and $v_a(G)$ at a range of volumes provided a means of fitting the hydrostatic deformation potentials, i.e., the volume derivatives of the band gaps. By inspecting the thus obtained ~20 discrete form factors, we found that v_s and v_a could each be fitted very well by a linear combination of two Gaussians. We were then able to reconstruct the atomic potentials $v_A = \frac{1}{2}(v_s + v_a)$ and $v_C = \frac{1}{2}(v_s - v_a)$ from the form factors. Each atomic pseudopotential $v_\alpha(q)$ is, therefore, a linear combination of four Gaussians, multiplied by a smooth function that allows adjustment of the small q components,

$$v_\alpha(q) = \Omega_\alpha \sum_{i=1}^{4} a_{i\alpha}\, e^{-c_{i\alpha}(q-b_{i\alpha})^2}\left[1 + f_{o\alpha}e^{-\beta_\alpha q^2}\right]. \quad (3)$$

Here, Ω_α is an atomic normalization volume. The qualitative shape of Eq. (3) resembles analytic forms found previously.[11] In the next step, we allow all of the parameters of Eq. (3) to be adjusted independently (the original form factors v_s and v_a may thus change), fitting the properties (ii) to (iv) described in the Introduction. In particular, the AlAs/GaAs valence-band offset [requirement (ii)] is calculated in a long-period superlattice geometry and fitted to the measured $\Gamma_{15v}(\mathrm{GaAs}) - \Gamma_{15v}(\mathrm{AlAs}) = 0.50$ eV.[21] The valence-band offset is controlled by the parameters $f_{o\alpha}$ and β_α in Eq. (3). The present EPM yields a work function[22] of 5.5 eV for GaAs, compared with the measured value of 5.56 eV for the (110) surface.[23] Concerning requirement (iii), we have found that a good fit to the s-orbital binding-energy differences of the *free Al and Ga pseudoatoms* is crucial for obtaining correct level splittings and thus band gaps in short-period superlattices. Therefore, rather than fitting level splittings in superlattices directly, we have solved the Schrödinger equation for the free Al and Ga pseudoatoms, and adjusted the parameters in Eq. (3) until we found good agreement with the s-orbital energy *difference* obtained with LDA, under the constraint that the previously fitted bulk properties do not change. We note that the s-orbital energy is mostly controlled by the core region of $v_\alpha(\boldsymbol{r})$, i.e., by the tail of $v_\alpha(\boldsymbol{q})$. Usually, empirical potentials are designed to be used with rather small $\boldsymbol{G}$-space cutoffs;[24] however, it is difficult to control the core region of the real-space atomic potential if too small a cutoff is used. Our parametrization of $v_\alpha(\boldsymbol{G})$ [Eq. (3)] allows us to independently adjust small-$\boldsymbol{G}$ and large-$\boldsymbol{G}$ regions of the potential.

As mentioned in the Introduction, we do not constrain the As pseudopotentials in AlAs and GaAs to be identical, thus, we account for the different charge transfer in the two materials: After fitting independently the As pseudopotentials in GaAs and AlAs [denoted as $v_{\mathrm{As}}(\mathrm{GaAs})$ and $v_{\mathrm{As}}(\mathrm{AlAs})$, respectively], the pseudopotential for As coordinated by $(4-n)$ Ga atoms and n Al atoms is taken as the weighted average [see Eq. (2)]

$$v_{\mathrm{As}}(\mathrm{Ga}_{4-n}\mathrm{Al}_n\mathrm{As}) = \frac{4-n}{4}v_{\mathrm{As}}(\mathrm{GaAs}) + \frac{n}{4}v_{\mathrm{As}}(\mathrm{AlAs}). \quad (4)$$

Note that this As potential only depends on the *number* of Ga and Al nearest neighbors and not on the *orientation* of the tetrahedron in a crystal. The orientation dependence enters through higher-order neighbor shells and is neglected in the present nearest-neighbor model.

The optimized parameters of Eq. (3) are given in Table I. The resulting bulk band gaps, deformation potentials, and effective masses are summarized in Table II, where we compare the present EPM band structures[24] of zinc blende GaAs and AlAs with experimental results[25–39] and theoretical calculations.[40,41] We obtain an excellent fit of the s-like conduction-band edges at the high symmetry points Γ, X, and L, whereas the p-like Γ_{15c} states are by ~ 0.7 eV too low in energy. The inclusion of nonlocal pseudopotentials is needed if a better agreement of the high-energy conduction bands is desired.[9] The deformation potentials agree with experiment within about 2 meV/kbar, and the sign of the small, but negative X-edge deformation potential is reproduced correctly. Comparison of the calculated band effective masses with experiment is not straightforward, because at this stage our EPM neglects spin-orbit interaction (see, however, below). We have converted the experimental hole effective masses to the nonrelativistic band structure using a $\boldsymbol{k}\cdot\boldsymbol{p}$ expansion around the Γ point, and compare the results with the EPM calculation in Table II. The deviation from the experimental values can be as much as 50% (for the Γ_{1c} electron effective mass), and as small as 2% (for

TABLE I. Atomic pseudopotential parameters [Eq. (3)], in Rydberg units, and Ω in atomic units. The four rows for each atom correspond to the four Gaussians $i = 1, 2, 3, 4$ in Eq. (3). We use $f_{o,\mathrm{Al}} = 0.02$, $\beta_{\mathrm{Al}} = 10$ (a.u.)$^{-1}$, and $f_{o,\mathrm{Ga}} = f_{o,\mathrm{As}} = 0$. The maximum momentum q we included in our calculation is 3.53 a.u., and the plane-wave kinetic-energy cutoff for which these potentials are designed is 5 Ry. A relativistic version is given in Table V.

Ω_α (a.u.)^3	$a_{i\alpha}$ Ry	$b_{i\alpha}$ (a.u.)$^{-1}$	$c_{i\alpha}$ (a.u.)^2
Al			
111.3	−1.32712	0	1.59819
	0.158114	1.77453	2.10827
	0.0601648	2.59550	0.527745
	0.0168167	2.93581	11.2708
Ga			
131.4	−1.24498	0	1.52748
	0.0366517	2.09782	0.959082
	0.0464357	2.01935	0.574047
	−0.0133385	2.93581	11.2708
As (in AlAs)			
145.2	−1.10411	0	0.972439
	0.0174946	2.46793	6.53147
	−0.00368081	1.22845	5.50601
	0.0921512	1.35897	1.18638
As (in GaAs)			
145.2	−1.05821	0	0.959327
	−0.00217627	2.46808	6.53145
	−0.0434312	0.851644	2.94679
	0.10569	1.22436	0.820922

the parallel electron mass at the X valley). The overall quality of the EPM fit to the bulk electronic properties is very satisfactory, and thus establishes requirement (i) of the introduction. In the appendix, we describe how spin-orbit interaction can be included in the present approach, and we also give the relevant parameter sets corresponding to Table I. In the applications below and in Sec. IV, however, we have neglected the spin-orbit interaction.

To demonstrate the quality of the present EPM in ternary compounds, we compare in Table III the calculated band gaps of $(\mathrm{AlAs})_n/(\mathrm{GaAs})_n$ (001) superlattices with experiment[42,43] and other theories.[44,45] Although the present potentials are aimed at a large variety of AlAs/GaAs nanostructure applications, short-period superlattices provide a stringent test of the transferability of the potentials, because they provide different local atomic environments, and the interfaces have a nonnegligible effect on the band structure. The established electronic properties of ideal-structure short-period $(\mathrm{AlAs})_n/(\mathrm{GaAs})_n$ superlattices along [001] are (i) an L-like conduction-band minimum (CBM) of the $n = 1$ superlattice,[44–47] (ii) an X-like indirect (at $X_{x,y}$) or pseudodirect (at X_z) CBM for $1 < n \leq 4$,[42] and (iii) a type-II to type-I transition at $n \approx 11$.[43] Furthermore, (iv) we compare the EPM wave functions and level splittings of [001] and [111] superlattices with LDA calculations. The present EPM reproduces these "benchmark" properties quite well:

(i) We find the conduction-band minimum in the abrupt $(\mathrm{AlAs})_1/(\mathrm{GaAs})_1$ (001) superlattice to be at the L point of the fcc Brillouin zone ($\bar{R}$ point in the tetragonal Brillouin zone), in agreement with quasiparticle[44] and LDA-corrected[45–48] calculations. This result is nontrivial, since in this superlattice the conduction band is strongly localized on the Ga sublattice; simple, bulklike pseudopotentials tend, in turn, to erroneously produce a delocalized, *mixed* (Al-Ga) CBM state, much like in the alloy. We will address this problem in more detail in Sec. IV A below.

(ii) For small n superlattices, where $1 < n \leq 8$, we obtain a pseudodirect or indirect gap, i.e., the conduction-band minimum originates either from the X_z or the $X_{x,y}$ states. This is in good agreement with LDA-corrected *ab initio* calculations[45] and with experiment,[42,43] when accounting for small strain effects that are neglected in the present calculation.[49]

(iii) The crossover between a pseudodirect band gap to a GaAs-like direct band gap (and hence, from type II to type I) is calculated to take place at $n \approx 9$. Experimentally, the crossover is found[43] at $n = 11 \pm 1$.

(iv) Whereas it is easy to reproduce by the EMA the wave functions of *long-period* superlattices, it is difficult to do so for short periods. In this regime the interfaces occupy a large fraction of the total superlattice volume, whereas in long-period superlattices this fraction becomes very small. The present pseudopotentials yield wave functions that closely resemble the LDA results even for short-period superlattices. This is illustrated in Figs. 1 and 2 that show contour plots of the wave functions squared of the $(\mathrm{AlAs})_1/(\mathrm{GaAs})_1$ superlattices oriented along [111] and along [001], respectively, as obtained from a self-consistent LDA calculation and the present EPM, respectively. (The contour level spacings are the same in both cases.) Note the strong non-effective-mass behavior of the two Γ-like conduction states shown in Fig. 1: one state is localized on the Ga (111) planes ($\bar{\Gamma}_{1c}^{(1)}$) and the other ($\bar{\Gamma}_{1c}^{(2)}$) is localized on the Al(111) planes. This segregation reflects the strong level repulsion of the zinc blende states Γ_{1c} and L_{1c}, leading to a $\bar{\Gamma}_{1c}^{(2)} - \bar{\Gamma}_{1c}^{(1)}$ energy separation of about 1 eV. Similarly, in the [001] superlattice, both the Γ-like and L-like conduction states depicted in Fig. 2 are localized on the Ga(001) planes. This wave function segregation and level repulsion is a crucial test for any empirical potential that is designed for systems with relatively small repeat unit cells, because poor wave functions and potentials can lead to wrong wave function coupling. In fact, while fitting our potentials we often found parameters that reproduced the bulk GaAs and AlAs band structure very well, and yet produced a CBM in the $(\mathrm{AlAs})_1/(\mathrm{GaAs})_1$ [111] superlattice that was localized on the *Al planes*, rather than on the *Ga planes*.

III. COMPARISON WITH PREVIOUS PSEUDOPOTENTIALS

The construction of previous potentials required (1) fitting of atomic form factors $v_\alpha(G)$ [see Eq. (1)] or crystal-

potential form factors $V(G)$ at the *bulk* reciprocal lattice vectors $\boldsymbol{G}_{\mathrm{ZB}}$, and (2) specification of the method used for obtaining form factors at lattice vectors $\boldsymbol{q}$ that are not zinc blende reciprocal vectors (e.g., whether small-q form factors were *fitted*, rather than extrapolated). Note that for a fit of small-q components one must use crystal structures that have large unit cells. Table IV provides an overview of some key features of previously proposed EPM's for AlAs/GaAs.[12–16] Results of a "performance test" for the monolayer $(\mathrm{AlAs})_1/(\mathrm{GaAs})_1$ [001] superlattice are also shown. The main differences between most of these methods and our approach are (1) we use a continuous, algebraic reciprocal-space form that is *fitted* to intermediate q values, rather than *interpolated*, (2) we use an environment-dependent As potential, (3) we find agreement of EPM superlattice wave functions with LDA-calculated ones, and (4) we fit *many* bulk properties, not just the band structure.

The first extension of the bulk EPM to AlAs/GaAs superlattices was performed by Caruthers and Lin-Chung.[12] They used a table of atomic form factors $v_\alpha(q)$ for α = Ga, Al, and As (with a single As potential), adjusting the Ga and Al form factors to fit the GaAs and AlAs band structures, respectively. The resulting $(\mathrm{AlAs})_1/(\mathrm{GaAs})_1$ [001] superlattice had a quasidirect gap $\bar{\Gamma}_{4c}(X_z)$ of 1.585 eV,[12] i.e., ~0.5 eV below the experimental or theoretical values given in Table III. Furthermore, the symmetry (X type instead of L type) is incorrect.

Andreoni *et al.*[13] have later suggested that the difference $\Delta v = v_{\mathrm{Ga}} - v_{\mathrm{Al}}$ ["scattering strength" in requirement (iii) of Sec. I above] might have been overestimated in Ref. 12, leading to the too large level repulsion in the $n = 1$ superlattice. Andreoni *et al.* used discrete bulk form factors for AlAs and GaAs, and extrapolated the values of $\Delta v(q)$ to the additional superlattice reciprocal-lattice vectors $G_{\mathrm{NZB}} = |\boldsymbol{G}_{\mathrm{SL}}|$. Because Δv in Ref. 13 was much smaller than that in Ref. 12, the superlattice band structure obtained in Ref. 13 resembled in fact the

TABLE II. Comparison of the electronic structure of bulk GaAs and AlAs as obtained in the present nonrelativistic EPM (Ref. 24), experiment, and *ab initio* theory. The zero of energy is at Γ_{15v}, the top of the valence band. Hydrostatic deformation potentials are given in meV/kbar. The GaAs experimental cyclotron effective masses have been converted to the nonrelativistic band structure using $\boldsymbol{k}\cdot\boldsymbol{p}$ theory. The electron effective masses at the X valley are given as $m_\parallel$ and $m_\perp$ along and perpendicular to the Δ axis, respectively. For analogous *relativistic* results, see Table VI.

Property	GaAs			AlAs		
	Present	Experiment	*Ab initio*	Present	Experiment	*Ab initio*
Energy levels (eV)						
Γ_{1v}	−12.12	−13.10[a]	−12.77[d]	−11.68		−11.93[d]
Γ_{1c}	1.52	1.52[b]	1.47[e]	3.04	3.13[f]	3.26[e]
Γ_{15c}	4.01	4.72[a]	4.52[e]	4.21	4.34[g]	5.05[e]
X_{5v}	−2.33	−2.80[a]	−2.73[e]	−2.29	−2.31[f]	−2.34[e]
X_{1c}	2.00	1.98[c]	2.08[e]	2.24	2.23[f]	2.09[e]
X_{3c}	2.32	2.38[c]	2.30[e]	3.04	2.68[f]	2.99[e]
L_{3v}	−0.96	−1.30[a]	−1.11[e]	−0.94	−1.29[h]	−0.88[e]
L_{1c}	1.81	1.81[c]	1.82[e]	2.87	2.54[h]	3.03[e]
Deformation potentials (meV/kbar)						
$a(E_g[\Gamma])$	8.46	10.82[i]	10.3[d]	8.49		10.6[d]
$a(E_g[X])$	−2.51	−1.26[j],−1.8[k]	−2.2[d]	−3.04	−1.53[j]	−2.2[d]
$a(E_g[L])$	2.59	5.5[l]	3.9[d]	2.52		5.1[d]
Effective masses (m_o)						
at Γ:						
m_n	0.099	0.066[m]		0.179		
m_p (Δ_5 [100])	0.431	0.403[n]		0.457		
m_p (Δ_1 [100])	0.102	0.063[n]		0.171		
at $\Delta_{\min}$ or X:						
$m_\parallel$	2.02	1.98[o]		1.30		
$m_\perp$	0.25	0.37[o]		0.26	0.19[p]	
0.82–1.2[e,f]		1.49				

[a]Reference 25.
[b]Reference 26.
[c]Reference 27.
[d]LDA corrected, Ref. 40.
[e]Quasiparticle calculation, Ref. 41.
[f]Reference 35.
[g]Reference 36.
[h]Reference 37.
[i]Reference 28.
[j]Reference 29.
[k]Reference 30.
[l]Reference 31.
[m]Reference 32.
[n]Reference 33.
[o]Reference 34.
[p]Reference 38.

$Al_{0.5}Ga_{0.5}As$ alloy, treated in the virtual-crystal approximation. Therefore, the CBM of the $n = 1$ superlattice was a virtual-crystal-like X state, rather than an L state.

Gell and co-workers[15] constructed the potentials using the original discrete *bulk* form factors[9] of AlAs and GaAs. It is not clear how the potentials were extrapolated to the superlattice reciprocal lattice vectors $\boldsymbol{G}_{\mathrm{SL}}$. Applying these potentials to the monolayer ($n = 1$) superlattice along (001), they found a delocalized, X-like CBM state,[15] in contradiction to subsequent calculations,[44,45] showing an L-like CBM (localized on the Ga sublattice, see Fig. 2). The pseudodirect-to-direct transition of the (001) superlattice was calculated to be at $n_c \approx 8$ monolayers, in reasonable accord with experiment.

Ikonic *et al.*[16] also used *bulk* form factors of AlAs and GaAs to construct the superlattice potential: in their method the GaAs *bulk* EPM is used up to the interface, at which point the AlAs *bulk* EPM is switched on abruptly. No intermediate region is allowed. It can be shown that in reciprocal space this scheme amounts to convoluting the zinc blende potentials with a one-dimensional Kronig-Penney model. An analytic "interpolation formula" to superlattice reciprocal lattice vectors can thus be derived. The valence-band offset was accounted for by shifting the two bulk band structures with respect to each other. For the (001) superlattices an L-like CBM was obtained for all $n \lesssim 7$ (in contradiction with other modern calculations[14,44–46] for $n \neq 1$), whereas for $n \geq 8$ a Γ-like CBM was obtained. Thus, these authors predicted an *indirect-to-direct* crossover at $n_c = 8$. The pseudodirect $\bar{\Gamma}(X_z)$ state was found to be above the CBM for all periodicities n.

Another approach, similar to ours, was followed by Xia, who used continuous, parametrized functions for the pseudopotentials fitted to the bulk band structures and to the valence-band offset.[14] Xia used two different al-

TABLE III. Energy levels of high-symmetry conduction-band states in $(AlAs)_n/(GaAs)_n$ [001] superlattices calculated by the present EPM and compared with experiment (Refs. 42 and 43), quasiparticle (QP) (Ref. 44), and LDA-corrected (Ref. 45) results. The reference energy is the (spin-orbit- and crystal-field-averaged) valence-band maximum. The superlattice Brillouin zone points are denoted by an overbar, and the corresponding folded zinc blende points are given in parentheses. The minimum gap for each period n is indicated by a star. The $\boldsymbol{k}$-selection rule of the lowest optical transition is indicated in the eighth column. The spatial nature of the fundamental transition is given in the last column.

n	Method	Superlattice state (folding ZB state)					Minimum gap	SL
		$\bar{\Gamma}(\Gamma_{1c})$	$\bar{\Gamma}(X_z)$	$\bar{M}(X_{x,y})$	$\bar{R}/\bar{X}(L)$	$\bar{Z}(\Delta)$	($\boldsymbol{k}$ selection)	type
1	present	2.02	2.12	2.12	1.93*	2.73	indirect	
	expt.[a]	2.20	2.09	2.07*			indirect	
	QP	2.11	2.23	2.13	1.85*		indirect	
	LDA	2.06	2.22	2.16	1.95*		indirect	
2	present	2.15	2.10*	2.10	2.25	2.21	pseudodirect	
	expt.[a]	2.19	2.08	2.07*			indirect	
	QP	2.23	2.18	2.16*	2.34		indirect	type II
	LDA	2.21	2.09*	2.12	2.35		pseudodirect	
3	present	2.13	2.08*	2.08	2.12	2.09	pseudodirect	type II
	expt.[a]	2.18	2.06	2.05*			indirect	
	LDA	2.15	2.05*	2.08	2.19		pseudodirect	
4	present	2.08	2.02*	2.06	2.20	2.03	pseudodirect	type II
	expt.[a]	2.19	2.04*	2.06			pseudodirect	
5	present	2.05	1.98	2.03	2.10	1.97*	indirect[b]	type II
6	present	2.00	1.94	2.00	2.12	1.94*	indirect[b]	type II
	expt.[c]	2.03	1.92*					
8	present	1.91	1.88*	1.94	2.05	1.88	pseudodirect	type II
10	present	1.82*	1.85	1.90	1.99	1.83	direct	type I
12	present	1.77*	1.82	1.87	1.95	1.77	direct	type I
20	present	1.64*	1.77			1.64	direct	type I

[a]Reference 42.
[b]Indirect by less than 10 meV.
[c]Extrapolated to $T = 0$ K, from Ref. 43.

gebraic forms, one for the Ga, and one for the Al and As potentials. These functions were fitted to the discrete form factors of the bulk zinc blende solids. The L-like band gaps of the (001) $n \times n$ superlattices are not given in Ref. 14, and the pseudodirect-to-direct crossover is not determined. However, the Γ-like gap at $n = 10$ is still 110 meV above the X_z-like gap and by extrapolation the crossover will probably be well above the experimentally found value of $n \approx 11$.[43]

All of the previously constructed empirical pseudopotentials for AlAs/GaAs assumed a single As potential for both GaAs and AlAs, or used the two bulk band structures only. In short-period superlattices, however, a large fraction of the As atoms is located at the interfaces. We believe that a local-environment dependence of the As potential such as given in Eq. (4), is crucial for the EPM to accurately reproduce the band structure in this regime (see Table III). Furthermore, a correct band offset and good effective masses are important for large-period superlattices, and hence a correct prediction of the type-II to type-I transition.

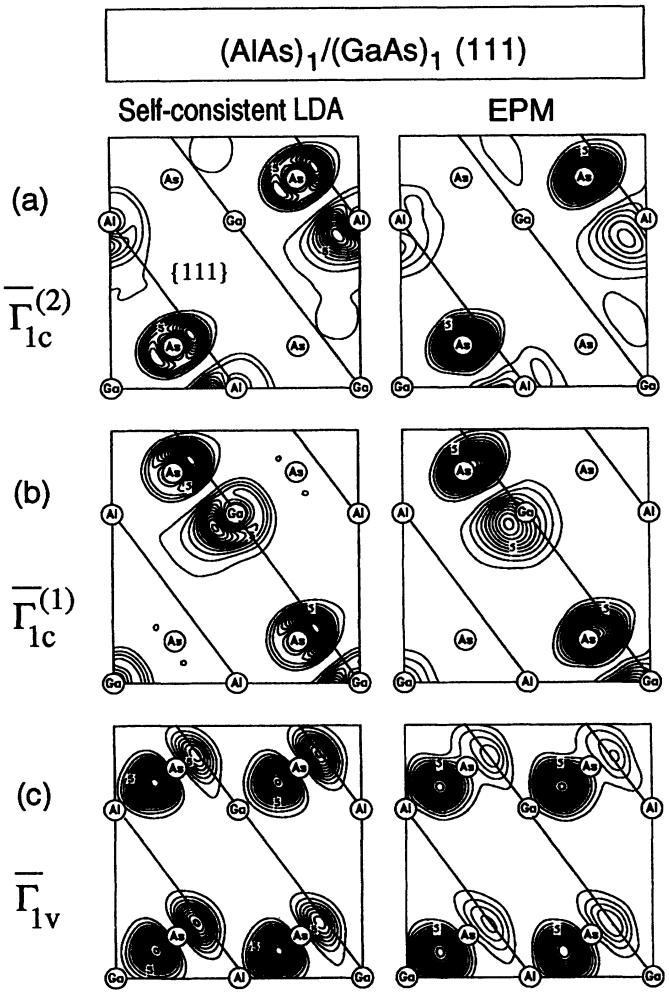

FIG. 1. Comparison of (a) $\bar{\Gamma}_{1c}^{(2)}$, (b) $\bar{\Gamma}_{1c}^{(1)}$, and (c) $\bar{\Gamma}_{1v}$ wave functions squared of the $(AlAs)_1/(GaAs)_1$ [111] superlattice (the "CuPt structure" $GaAlAs_2$) as obtained with the self-consistent LDA (left) and the empirical-pseudopotential method (right), respectively. We plot the results on the $(1\bar{1}0)$ plane using the same contour level spacings [1 electron/(a.u.)^3] for both the LDA and the EPM wave functions. Diagonal lines denote the {111} planes. $\bar{\Gamma}_{1v}$ is the nondegenerate crystal-field split state originating from the zinc blende Γ_{15v} states. It is below the doubly degenerate $\bar{\Gamma}_{3v}$ state by Δ_{CF}. $\bar{\Gamma}_{1c}^{(1)}$ and $\bar{\Gamma}_{1c}^{(2)}$ are the symmetry-repelled conduction states originating from Γ_{1c} and folded L_{1c}. Their splitting energy is 0.98 eV for LDA and 1.01 eV for EPM, respectively.

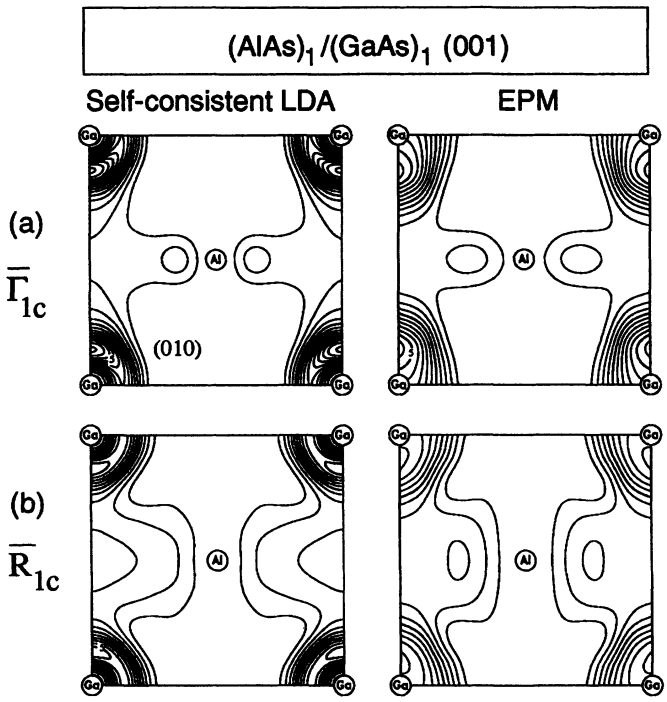

FIG. 2. Comparison of (a) $\bar{\Gamma}_{1c}$ and (b) $\bar{R}_{1c}$ wave functions squared of the $(AlAs)_1/(GaAs)_1$ [001] superlattice (the "CuAu structure" $GaAlAs_2$) as obtained with the self-consistent LDA (left) and the empirical-pseudopotential method (right), respectively. The results are shown in the (010) plane, using the same contour level spacings [0.5 electrons/(a.u.)^3] for both the LDA and the EPM wave functions. $\bar{R}_{1c}$ corresponds to the folded zinc blende L_{1c} state and is lower in energy than $\bar{\Gamma}_{1c}$.

IV. ILLUSTRATIVE APPLICATIONS

To apply the present EPM to very large systems, an efficient algorithm is needed to solve the Schrödinger equation with a fixed potential in a plane-wave basis. Such a scheme (the "folded-spectrum method"), whose computational effort scales *linearly* with the number of atoms in the supercell, was recently developed by Wang and Zunger.[8] We illustrate the utility of the present pseudopotentials by applying them with the folded-spectrum method to the calculation of the electronic structure of three prototypical systems that require large supercells with complex geometries. All calculations are done by expanding the wave functions in a plane-wave basis set with a cutoff of 5.0 Ry, evaluating exactly the matrix elements of our pseudopotentials and using the method of Ref. 8 for finding eigensolutions near the band edges.

TABLE IV. Comparison of previous EPM's with the present one. In the second column, the potential type is specified, i.e., "atomic," if atomic form factors are used [see Eq. (1)], "bulk," if the bulk potential of AlAs and GaAs is retained and an infinitesimal interface in AlAs/GaAs is assumed. Columns three to five indicate whether deformation potentials and the AlAs/GaAs band offset were fitted, and how $V(q)$ was obtained at those reciprocal vectors that are not zinc blende vectors $\boldsymbol{G}_{\rm ZB}$ (see text). The symmetry of the CBM of the $n = 1$ $(\mathrm{AlAs})_n/(\mathrm{GaAs})_n$ (001) superlattice is reported in the last column. Quasiparticle calculations (Ref. 44) place the $n = 1$ CBM at $\bar{R}(L)$.

Method	Potential type	Def. pot. fitted	$\Delta E_{\rm v}$ fitted	$V(q)$ at $q \neq G_{\rm ZB}$	(001) SL $n = 1$ CBM
Caruthers and Lin-Chung (Ref. 12)	$v_{\rm Ga}, v_{\rm Al}, v_{\rm As}$ atomic potentials	No	No	Interpolated	$\bar{\Gamma}(X_z)$
Andreoni *et al.* (Ref. 13)	$\Delta v = v_{\rm Ga} - v_{\rm Al}$ bulk/atomic	No	No	Interpolated	$\bar{\Lambda}(\Delta_z)$
Gell *et al.* (Ref. 15)	AlAs, GaAs bulk potentials	No	Yes		$\bar{\Gamma}(X_z)$
Xia (Ref. 14)	$v_{\rm Ga}, v_{\rm Al}, v_{\rm As}$ atomic potentials	No	Yes	Algebraic fit	$\bar{\Gamma}(X_z)$
Ikonic *et al.* (Ref. 16)	AlAs, GaAs bulk potentials	No	Yes	Convolution	$\bar{R}(L)$
Present	$v_{\rm Ga}, v_{\rm Al}$, $v_{\rm As}[\mathrm{Ga}_{4-n}\mathrm{Al}_n]$ atomic potentials	Yes	Yes	Algebraic fit supercells	$\bar{R}(L)$

A. Superlattices with chemical interfacial roughness

Chemical nonabruptness of interfaces in short-period superlattices has been suggested[47] as a reason for the discrepancy between the experimental assignment of the conduction-band minimum and theoretical predictions (see Table III). In particular, for the monolayer ($n = 1$) superlattice along (001), state-of-the-art quasiparticle calculations place the conduction-band minimum at the L-derived $\bar{R}$ point in the tetragonal Brillouin zone,[44] whereas experimentally a $X_{x,y}$-derived gap at $\bar{M}$ is found.[42] Using (2×1), (3×1), and (4×1) interfacial unit cells [where $(X \times Y)$ denotes the two-dimensional unit cell in the (001) plane spanned by the basis vectors $X\frac{a}{2}(110)$ and $Y\frac{a}{2}(1\bar{1}0)$], Laks and Zunger[47] showed that exchanging a fraction $f \gtrsim \frac{1}{3}$ of Ga and Al atoms across the interface changes the identity of the CBM in the monolayer superlattice from $\bar{R}(L)$ to $\bar{M}(X_{x,y})$. Thus the observed $\bar{M}(X_{x,y})$ CBM was interpreted as a consequence of interfacial roughness. However, because these calculations were performed within the LDA, rather small $(X \times Y \leq 4)$ interfacial unit cells were used.

The present EPM allows us to use much larger supercells, thus eliminating any size effects that could lead to artefacts in the band structure. The monolayer superlattice can be viewed as a partially ordered CuAu structure, i.e., it can be written as $(\mathrm{Al}_{x+\frac{\eta}{2}}\mathrm{Ga}_{x-\frac{\eta}{2}}\mathrm{As})_1/(\mathrm{Al}_{x-\frac{\eta}{2}}\mathrm{Ga}_{x+\frac{\eta}{2}}\mathrm{As})_1$, where η is the long-range order (LRO) parameter.[50] $\eta = 1$ denotes the ideal superlattice with abrupt interfaces, whereas $\eta = 0$ characterizes the random alloy. To simulate interfacial roughness in the monolayer superlattice we expand the repeat period $(X \times Y)$ in the interface plane to an (8×8) unit cell. We can thus have $\eta = 1 - n/32$, where n is the number of Ga/Al pairs interchanged accross the interface. In each cation layer, the Ga and Al atoms are randomly distributed on the lattice sites, hence there is in principle no periodicity along the growth axis [001]. For computational reasons, however, we assume a repeat period of four monolayers along [001], resulting in a 512-atom supercell. Hence, within the supercell there are four distinct Al-rich and four distinct Ga-rich layers, with compositions $0.5 + \eta/2$ and $0.5 - \eta/2$, respectively.

The energy eigenvalues of the large supercell are analyzed in terms of their "parent" zinc blende states from which they originate. Because zinc blende states are allowed to mix in the superlattice (subject to $\boldsymbol{k}$-selection and point-group selection rules), a superlattice wave function can be expanded in terms of a usually small number of zinc blende wave functions. We use the expansion coefficients of the latter expansion as weights in evaluating *spectral averages* of zinc-blende-like eigenvalues.[19] For example, $\langle \Gamma_{1c} \rangle$ denotes the expectation value of the zinc blende Γ_{1c} energy level in a given supercell. $\langle \Gamma_{1c} \rangle$, $\langle X_{1c} \rangle$, and $\langle L_{1c} \rangle$ are shown in Fig. 3 for $\eta = 0$, 0.25, 0.50, 0.75, and for the perfect monolayer superlattice ($\eta = 1$). Interpolation curves based on simple scaling laws[51] pertinent to LRO are shown as lines. We predict a transition from an X-like CBM to an L-like CBM at $\eta \approx 0.4$, in close agreement with the LDA result[47,50] ($\eta \approx \frac{1}{3}$). At $\eta = 1$, the spectral averages of the

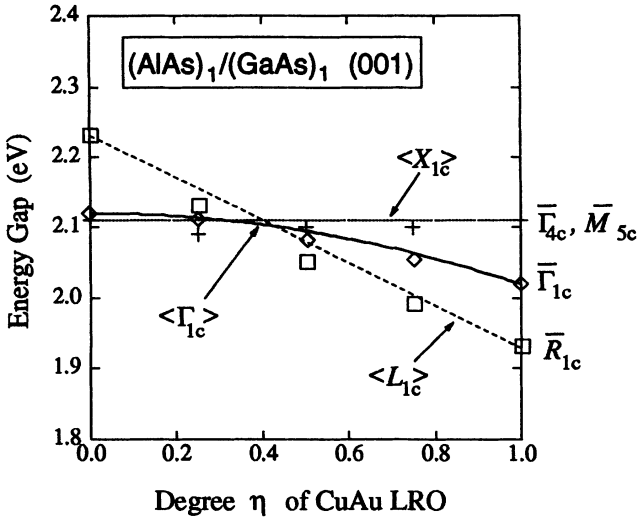

FIG. 3. Spectral averages of the zinc-blende-like Γ_{1c} (diamonds), X_{1c} (pluses), and L_{1c} (squares) energy gaps, respectively, plotted as a function of η, the degree of CuAu long-range order. The solid line is a quadratic interpolation between the $\eta = 0$ and $\eta = 1$ values of $\langle\Gamma_{1c}\rangle$ and the broken lines are linear interpolations between the respective endpoints of $\langle X_{1c}\rangle$ and $\langle L_{1c}\rangle$.

zinc blende states have definite tetragonal symmetry, i.e., $\langle\Gamma_{1c}\rangle \to \bar{\Gamma}_{1c}$, $\langle L_{1c}\rangle \to \bar{R}_{1c}$, and $\langle X_{1c}\rangle \to \bar{\Gamma}_{4c} + \bar{M}_{5c}$. Note that the latter two states, which derive from X_z and $X_{x,y}$, respectively, are almost degenerate in our EPM calculation, whereas experimental observation gives a splitting of 19 meV (see Table III). The fact that experimentally an X-like band gap at $\bar{M}$ is found,[42] is consistent with our calculation if the superlattice is only partially ordered with $\eta \lesssim 0.4$. From the figure it seems that we can rule out the possibility of a Γ_{1c}-like CBM at any η, because a correct $X_z - X_{x,y}$ splitting would push the $\bar{M}$-like level to even lower energy.

B. Disordered, short-period superlattices

Disordered superlattices (d-SL's) represent a one-dimensional sequence $A_nG_mA_{n'}G_{m'}A_{n''}G_{m''}\cdots$, where A and G denote AlAs and GaAs layers, respectively, and the individual layer thicknesses $n, m, n', m', \ldots$ are chosen at random. Short-period d-SL's are generated in practice[52] by restricting the layer thicknesses to a set of small numbers, e.g., $n, m \in \{1, 2, 3\}$ with occurrence probabilities $p(1), p(2), p(3)$. Such a superlattice, denoted d-SL(1,2,3), can be viewed as a randomization of an ordered A_2G_2 superlattice (o-SL), with fluctuations around the average layer thickness $n = m = 2$. Such superlattices were grown by Sasaki and co-workers using molecular-beam epitaxy (MBE) and their basic properties were measured.[52] The main experimental findings were: (i) a large redshift of the photoluminescence (PL) peak with respect to both the random $Al_{0.5}Ga_{0.5}As$ alloy and the o-SL, (ii) an enhanced PL intensity at higher temperatures, and (iii) shorter PL decay times.

Due to the absence of periodicity along the growth direction (001), we need very large supercells to realistically model the electronic structure of a d-SL. We have constructed a random sequence of 1000 monolayers, corresponding to a ~300 nm thick sample, which is comparable to the actual dimensions of molecular-beam-epitaxy grown d-SL's.[52] In the plane perpendicular to the growth axis we assumed perfect translational symmetry (2 atoms per cell), thus our overall three-dimensional supercell contains 2000 atoms. We have calculated the near-band-edge energy levels and wave functions of a d-SL(1,2,3) and show the VBM and CBM wave functions in Fig. 4.

Our results are as follows.

(i) The calculated energy gaps are 2.11, 2.10, and 1.94 eV for the random alloy, o-SL, and d-SL(1,2,3), respectively. The observed photoluminescence peak energies are 2.05, 2.02, and 1.96 eV for the respective systems.[52] The calculated energy gap of the d-SL is reduced by 170 meV with respect to the random alloy of equivalent composition and by 160 meV with respect to the o-SL.

(ii) The wave functions near the valence-band and conduction-band edges are strongly localized along the growth direction; they spread over ~25 monolayers and decay exponentially outside this region with decay lengths of 2–3 monolayers. Electrons and holes that are localized in the same region will recombine very quickly, because the wave function overlap and thus the oscillator strength is large. A more detailed account of our results will be presented in a future publication.

C. Substitutional isoelectronic impurity clusters

The study of very small quantum dots, or clusters, embedded in a crystalline host is another example where a

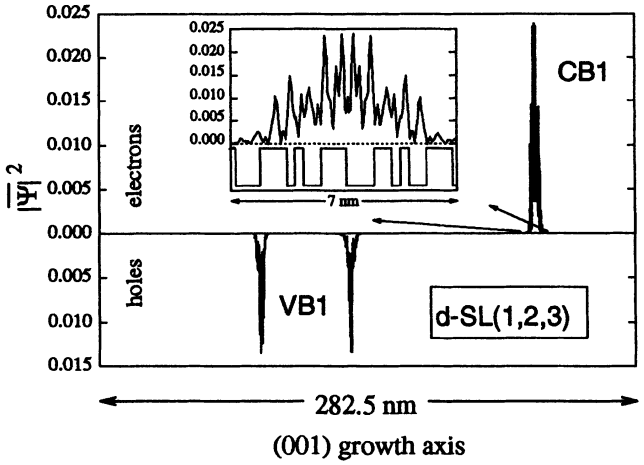

FIG. 4. Planar average of the wave function squared along the growth direction [001] of d-SL(1,2,3). The lowest conduction state (CB1) and the highest valence state (VB1) are shown. The latter is twofold degenerate, hence the two-peak structure. The wave functions are normalized to one. The inset shows a blown-up region around CB1, together with a schematic of the growth sequence of the d-SL. "Wells" denote GaAs layers and "barriers" denote AlAs layers. Both the well and barrier widths vary from one to three monolayers.

microscopic potential and at the same time large supercells are needed. The experimental feasability of such small nanostructures has been demonstrated recently, e.g., by intentional MBE growth of $In_{0.5}Ga_{0.5}As$ quantum dots embedded in GaAs,[53] and by unintentional formation of GaAs "quantum dots" at the AlAs/GaAs interface of AlAs/GaAs quantum wells.[54] We illustrate the usefulness of our present method for theoretical studies of embedded quantum dots by considering substitutional n-atom Ga_n clusters with idealized geometries in an AlAs host crystal, denoted AlAs:Ga_n, where n connected Al atoms are substituted by Ga atoms. It is known that a *single* Ga isoelectronic impurity ($n = 1$) in AlAs does not have a bound state in the energy gap.[55] Very large clusters may be described by the particle-in-a-box, or effective-mass model. In terms of the effective-mass picture, a GaAs quantum dot in AlAs acts as a quantum well with a potential depth of about 1 eV. The minimum size of a spherical quantum dot above which effective-mass theory predicts a bound electron can easily be calculated to be $n \approx 160$. However, the CBM of AlAs is at the X point in the Brillouin zone rather than at the Γ point, hence quasibound states with small binding energies can lie in the continuum of the AlAs conduction bands and will form *resonant* states even for very small cluster sizes. An analogous situation occurs in the case of ultrathin GaAs quantum wells in AlAs, where it was calculated that for (001) quantum wells with thickness d smaller than 11 monolayers, the quantum-well states are resonant with the AlAs conduction bands, and only for $d \geq 11$ do bound electrons below the CBM exist.[56] In the case of a spherical quantum dot, a simple effective-mass calculation gives a cluster size of $n \approx 4200$ above which a bound electron exists below the AlAs X edge. Here, we are interested in much smaller cluster sizes, where resonant electron states are expected.

To simulate a Ga_n cluster in an AlAs host, we use a cubic supercell containing 512 atoms, which is sufficiently large to prevent interaction between the periodically repeated clusters for small n. We then replace $n = 1$, 4, and 14 Al atoms by Ga, taking the shape of cubic cluster geometries, i.e., for $n = 4$ we have a tetrahedron and for $n = 14$ we have a cube. We can classify the eigenstates of the systems according to molecular orbitals of cubic point symmetry. In Fig. 5 we plot the near-band-edge spectra of the substitutional clusters as a function of the effective supercell composition $x = n/256$. For all clusters considered, we find the lowest unoccupied state to be an X-derived threefold degenerate t_2 level. This state is clearly not effective-mass-like. In fact, inspection of the wave function for $n = 14$ reveals that this t_2 state is AlAs-like, i.e., it is extended in the AlAs region and slightly attenuated in the GaAs cluster. Therefore, we identify this state with the true, AlAs-like CBM of the system, even though it lies by ~30 meV below the bulk AlAs CBM (see Fig. 5). This apparent "binding energy" of 30 meV has in fact a contribution from the hole binding energy of ~20 meV. (Note that in Fig. 5 the zero of energy is at the VBM of the impurity system.) The remaining shift (~10 meV) is probably due to the onset of interaction between Ga_{14} clusters in neighboring

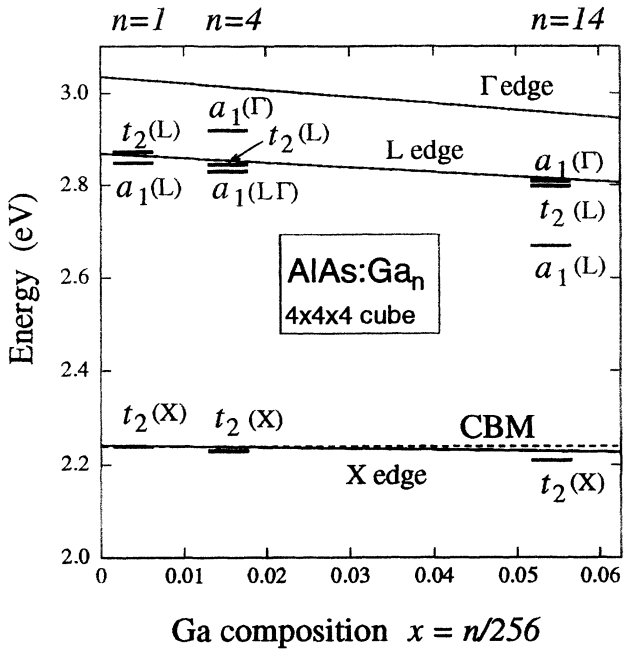

FIG. 5. Energy levels of a Ga_n cluster in an AlAs host, simulated by a 512 atom cubic supercell. The abscissa denotes the effective stoichiometry of the supercell, when n Al atoms are substituted by Ga atoms. Solid lines indicate the band gaps as a function of the effective composition x, neglecting optical bowing. The dashed line denotes the X-like conduction-band minimum of the AlAs host. Due to the cubic symmetry of the system, the three X_{1c} states give rise to threefold degenerate t_2 levels, whereas the four L_{1c} states split into $t_2 + a_1$, and the Γ_{1c}-derived states have a_1 symmetry.

supercells. The Γ- and L-derived states appear as resonances in the conduction band of the AlAs host. In the largest cluster ($n = 14$), these resonances are about 150 meV lower in energy than their "parent states." Note that this appreciable resonance energy occurs for a cluster size well below the minimum cluster size $n \approx 160$ for which effective-mass theory predicts the occurrence of a "bound" state with zero binding energy. Of course, for $n \to \infty$, the lowest unoccupied state would be the bulk-GaAs Γ_{1c} level, hence at some finite $n > 14$ the $a_1(\Gamma)$ resonance evolves into a bound state below the AlAs CBM. However, larger supercells are needed to study clusters with $n > 14$ and the best estimate of the critical cluster size remains the effective-mass value of $n \approx 4200$.

V. SUMMARY

We presented empirical pseudopotentials for Ga, Al, and As that can be used in a large variety of atomic environments in AlAs/GaAs ternary systems. The main features of the potentials are (i) a continuous, algebraic form $v_\alpha(q)$ for the atoms α = Al, Ga, and As, (ii) an explicit dependence of the As potential on the number of Ga and Al nearest neighbors, (iii) a good fit to the bulk AlAs and GaAs electronic properties, (iv) a good fit to LDA-calculated level splittings in short-

TABLE V. Same as Table I, when spin-orbit interaction is included [Eq. (A1)]. $f_{o,\mathrm{Al}} = 0.02$, $\beta_{\mathrm{Al}} = 10$ (a.u.)$^{-1}$, and $f_{o,\mathrm{Ga}} = f_{o,\mathrm{As}} = 0$ [see Eq. (3)] remain unchanged. The cutoff radius for the spin-orbit potential in Eq. (A2) is $r_c = 2$ a.u. for all atom types, and $\lambda_\alpha = \lambda_{\alpha,l=1}$ is given in the first column below the atomic volume.

Ω_α (a.u.)^3 λ_α (Ry)	$a_{i\alpha}^{so}$ Ry	$b_{i\alpha}^{so}$ (a.u.)$^{-1}$	$c_{i\alpha}^{so}$ (a.u.)^2
Al			
111.3	−1.32512	0	1.60516
	0.137042	1.7575	2.10803
$\lambda_{\mathrm{Al}} = 0$	0.00877023	2.5963	0.527774
	0.0231561	2.9377	11.2707
Ga			
131.4	−1.22489	0	1.51845
	0.0438261	2.11885	0.959082
$\lambda_{\mathrm{Ga}} = 0.2453$	0.0565582	2.02596	0.581972
	−0.0108889	2.94278	11.2711
As (in AlAs)			
145.2	−1.14809	0	0.971094
	0.0187039	2.46814	6.53134
$\lambda_{\mathrm{As}} = 0.294$	0.00613087	1.23022	5.50596
	0.0979212	1.36895	1.18829
As (in GaAs)			
145.2	−1.07477	0	0.963769
	−0.0146395	2.46945	6.53143
$\lambda_{\mathrm{As}} = 0.294$	−0.0512007	0.837519	2.94696
	0.111554	1.22457	0.824441

period $(\mathrm{AlAs})_n/(\mathrm{GaAs})_n$ superlattices. The wave functions obtained with the present EPM are very similar to LDA-calculated wave functions. For short-period superlattices, the present pseudopotentials represent a significant improvement over previous ones, which typically fail to reproduce the LDA-calculated energy-level order in short-period superlattices. We have applied our pseudopotentials to large systems with complex geometries, i.e., superlattices with rough interfaces, disordered short-period superlattices, and isoelectronic impurity clusters. The supercells needed for their simulation contained up to 2000 atoms. We expect that these new pseudopotentials can be used in realistic calculations of quantum structures, whenever effective-mass approximations are inappropriate.

ACKNOWLEDGMENTS

This work was supported by the Office of Energy Research, Materials Science Division, U.S. Department of Energy, under Grant No. DE-AC02-83CH10093.

APPENDIX: SPIN-ORBIT INTERACTION

The spin-orbit interaction can be added to the present method in the form of an atomic difference potential for a given orbital quantum number l,

TABLE VI. Comparison of critical point energies of bulk GaAs and AlAs as obtained in the present relativistic EPM (using the parameters of Table V and spin-orbit interaction) with experiment. The zero of energy is at Γ_{8v}, the top of the valence band.

Label	GaAs		AlAs	
	Present	Experiment	Present	Experiment
Γ_{6v}	−12.22	−13.10[a]	−11.80	
Δ_0	0.34	0.34[b]	0.31	0.28[e]
Γ_{6c}	1.52	1.52[c]	3.05	3.13[f]
Γ_{7c}	3.74	4.49[b]	4.36	4.34[e]
Δ_0'	0.19	0.17[b]	0.04	
X_{7v}	−2.41	−2.80[a]	−2.25	−2.31[f]
$\Delta_2(X)$	0.08	0.08[b]	0.15	0.15[e]
X_{6c}	1.94	1.98[d]	2.27	2.23[f]
X_{7c}	2.33	2.38[d]	2.85	2.68[f]
$L_{4,5v}$	−0.98	−1.30[a]	−0.91	−1.29[g]
Δ_1	0.21	0.22[b]	0.18	0.20[e]
L_{6c}	1.80	1.81[d]	2.82	2.54[g]
Effective masses at Γ (m_o):				
m_n	0.092	0.066[h]	0.156	
m_{hh}	0.394	0.450[i]	0.459	
m_{lh}	0.134	0.082[i]	0.208	
m_{so}	0.189	0.170[j]	0.302	

[a]Reference 25. [f]Reference 35.
[b]Reference 59. [g]Reference 37.
[c]Reference 26. [h]Reference 32.
[d]Reference 27. [i]Reference 33.
[e]Reference 36. [j]Reference 39.

$$v^{so}_{\alpha,l}(r) = \frac{2}{2l+1}\left[v_{\alpha,l+\frac{1}{2}}(r) - v_{\alpha,l-\frac{1}{2}}(r)\right], \qquad \text{(A1)}$$

where $j = l \pm \frac{1}{2}$ is the total angular momentum resulting from the spin-orbit coupling, and $v_{\alpha,j}$ is the pseudopotential of atom α acting on the (atomic) pseudowave function with angular momentum j.[57] Equation (A1) is then included for each atom in the crystal potential in Eq. (1). We have implemented the resulting nonlocal part of the potential using the scheme of Kleinman and Bylander,[58] which approximates the fully nonlocal operator in reciprocal space by a separable one, thus reducing the computational cost considerably. We use a two-parametric analytic form to model Eq. (A1), which is positive within a small cutoff radius r_c, and zero elsewhere. For $r \leq r_c$, we choose a zero-order spherical Bessel function, truncated at its first minimum, i.e.,

$$v^{so}_{\alpha,l}(r) = \lambda_{\alpha,l}\left[\frac{\sin\gamma r}{\gamma r} - \frac{\sin\gamma r_c}{\gamma r_c}\right], \quad r \leq r_c, \qquad \text{(A2)}$$

where γ is the smallest positive root of $\gamma r_c = \tan\gamma r_c$. The shift in Eq. (A2) makes the spin-orbit potential positive for $r < r_c$, and continuous at $r = r_c$. From relativistic atomic LDA calculations we know that $r_c = 2$ a.u. (and $\gamma = 2.2467$ a.u.$^{-1}$) is a reasonable choice, and we have then used $\lambda_{\alpha,l=1}$ as a single parameter to fit the experimental spin-orbit splittings in zinc blende GaAs and AlAs. We neglect spin-orbit interaction for $l > 1$.

Note that the parameters in Table I were obtained by fitting the EPM band structure without spin-orbit coupling to experimental band extrema, thus mimicking a *relativistic* band structure. For example, the Γ_{15v} level was fitted to the experimental Γ_{8v} level, thus neglecting the split-off Γ_{7v} state. Adding the spin-orbit interaction to the nonrelativistic potential without modification of the parameters would, therefore, distort the band structure. We have found that small adjustments of the parameters in Table I suffice to fit the relativistic band structure with equal quality like the nonrelativistic fit shown in Table II (with obvious changes from single-group to double-group notation). The modified parameters, to be used when spin-orbit interaction is included, are given in Table V. The resulting band gaps and spin-orbit splittings are shown in Table VI. The experimental spin-orbit splittings can be fitted within less than 10% with the simple two-parametric model potential of Eq. (A2).

When spin-orbit coupling is included, the computational effort approximately quadruples, since both the number of bands and the spin degrees of freedom are doubled. For large supercells, however, a nonrelativistic calculation can first be performed, and the spinors constructed from the spin-less eigenfunctions (e.g., exact eigenstates of σ_z) provide an excellent first guess for the relativistic eigenfunctions. We have found that with our conjugate-gradient code one to two additional iterations usually suffice to find the correct relativistic eigenfunctions. Finally, we point out that the inclusion of an l-dependent potential (spin-averaged potential of orbital quantum number l) adds no extra cost, when spin-orbit interaction is included, because in the Kleinman-Bylander scheme the latter is already treated as a (spin-dependent) nonlocal potential.[58] A p potential that is different from the s potential may improve certain details of the band structure (see discussion in Sec. II), but in the present work we have used the same local potential for $l = 0$ and $l = 1$.

[1] A. Zunger and S. Mahajan, *Handbook on Semiconductors*, 2nd ed. (Elsevier, Amsterdam, 1994), Vol. 3, p. 1399.

[2] A. Ourmazd, D. W. Taylor, J. Cunningham, and C. W. Tu, Phys. Rev. Lett. **62**, 933 (1989).

[3] See, for example, ***Microcrystalline Semiconductors: Materials Science and Devices*, edited by P. M. Fauchet, C. C. Tsai, L. T. Canham, I. Shimizu, and Y. Aoyagi, MRS Symposia Proceedings No. 283 (Materials Research Society, Pittsburgh, 1993).**

[4] G. Bastard, *Wave Mechanics Applied to Semiconductor Heterostructures* (Les Éditions de Physique, Les Ulis, France, 1988).

[5] Z. Q. Li and W. Pötz, Phys. Rev. B **46**, 2109 (1992).

[6] S. Y. Ren and J. D. Dow, Phys. Rev. B **45**, 6492 (1992).

[7] P. E. Lippens and M. Lannoo, Mater. Sci. Eng. **B 9**, 485 (1991).

[8] L.-W. Wang and A. Zunger, J. Chem. Phys. **100**, 2394 (1994).

[9] M. L. Cohen and J. R. Chelikowsky, *Electronic Structure and Optical Properties of Semiconductors* (Springer-Verlag, Berlin, 1988).

[10] M. L. Cohen and T. K. Bergstresser, Phys. Rev. **141**, 789 (1966).

[11] M. L. Cohen and V. Heine, in *Solid State Physics, Advances in Research and Applications*, edited by H. Ehrenreich, F. Seitz, and D. Turnbull (Academic Press, New York, 1970), Vol. 24, p. 38.

[12] E. Caruthers and P. J. Lin-Chung, Phys. Rev. B **17**, 2705 (1978).

[13] W. Andreoni, A. Baldereschi, and R. Car, Solid State Commun. **27**, 821 (1978).

[14] J.-B. Xia, Phys. Rev. B **38**, 8358 (1988).

[15] M. A. Gell, D. Ninno, M. Jaros, and D. C. Herbert, Phys. Rev. B **34**, 2416 (1986).

[16] Z. Ikonic, J. C. Inkson, and G. P. Srivastava, Semicond. Sci. Technol. **7**, 648 (1992); G. P. Srivastava (private communication).

[17] R. Magri, S.-H. Wei, and A. Zunger, Phys. Rev. B **42**, 11 388 (1990), and references therein.

[18] Z. W. Lu, S.-H. Wei, A. Zunger, S. Frota-Pessoa, and L. G. Ferreira, Phys. Rev. B **44**, 512 (1991).

[19] K. A. Mäder and A. Zunger (unpublished).

[20] P. Friedel, M. S. Hybertsen, and M. Schlüter, Phys. Rev. B **39**, 7974 (1989).

[21] D. J. Wolford, in *Proceedings of the 18th International Conference on the Physics of Semiconductors, Stockholm, 1986*, edited by O. Engström (World Scientific, Singapore, 1987), p. 1115.

[22] Note that because the EPM uses screened atomic potentials, the absolute reference energy of the solid is simply that of the free atom.
[23] J. van Laar, A. Huijser, and T. L. van Rooy, J. Vac. Sci. Technol. **14**, 894 (1977).
[24] We have used a kinetic-energy cutoff for the plane-wave basis of 5.0 Ry, resulting in about 30 plane waves per atom. The potential $V(\boldsymbol{r})$ was discretized on a simple-cubic grid with a resolution $\Delta r = a/12$, where $a = 10.68$ a.u. is the GaAs and AlAs lattice constant. This grid resolution corresponds to a maxium momentum q in reciprocal space of 3.53 a.u.$^{-1}$.
[25] T. C. Chiang, J. A. Knapp, M. Aono, and D. E. Eastman, Phys. Rev. B **21**, 3513 (1980).
[26] D. D. Sell, Phys. Rev. B **6**, 3750 (1972).
[27] D. E. Aspnes, C. G. Olson, and D. W. Lynch, Phys. Rev. Lett. **37**, 766 (1976).
[28] A. R. Goñi, K. Syassen, K. Strössner, and M. Cardona, Semicond. Sci. Technol. **4**, 246 (1989).
[29] K. Reimann, M. Holtz, K. Syassen, Y. C. Lu, and E. Bauser, Phys. Rev. B **44**, 2985 (1991).
[30] D. Olego, M. Cardona, and H. Müller, Phys. Rev. B **22**, 894 (1980).
[31] A. Azema, J. Botineau, F. Gires, and A. Saissy, J. Appl. Phys. **49**, 24 (1987).
[32] J. M. Chamberlain, P. E. Simmonds, R. A. Stradling, and G. G. Bradley, in *Proceedings of the 11th International Conference on Physics of Semiconductors, Warsaw, 1972*, edited by M. Miasek (PWN-Polish Scientific, Warsaw, 1972), p. 1016.
[33] M. S. Skolnick, A. K. Jain, R. A. Stradling, L. Leotin, J. C. Ousset, and S. Ashkennazy, J. Phys. C **9**, 2809 (1976).
[34] A. F. Kravchenko, W. S. Sardarjan, and W. W. Efimov, in *Proceedings of the 8th International Conference on Physics of Semiconductors, Kyoto, 1966* (Physical Society of Japan, Tokyo, 1966), p. 346.
[35] B. Monemar, Phys. Rev. B **8**, 5711 (1973).
[36] A. Onton, in *Proceedings of the 10th International Conference on Physics of Semiconductors, Cambridge, Massachusetts, 1970* (USAEC, New York, 1970), p. 107.
[37] D. E. Aspnes, S. M. Kelso, R. A. Logan, and R. Bhatt, J. Appl. Phys. **60**, 754 (1986).
[38] B. Rheinländer, H. Neumann, P. Fischer, and G. Kühn, Phys. Status Solidi B **48**, K167 (1972).
[39] A. L. Mears and R. A. Stradling, J. Phys. C **4**, L22 (1971).
[40] S.-H. Wei and A. Zunger, Phys. Rev. B **39**, 3279 (1989).
[41] R. W. Godby, M. Schlüter, and L. J. Sham, Phys. Rev. B **35**, 4170 (1987).
[42] W. Ge, W. D. Schmidt, M. D. Sturge, L. N. Pfeiffer, and K. W. West, J. Lumin. **59**, 163 (1994).
[43] G. Li, D. Jiang, H. Han, Z. Wang, and K. Ploog, Phys. Rev. B **40**, 10 430 (1989).
[44] S. B. Zhang, M. L. Cohen, S. G. Louie, D. Tomanek, and M. S. Hybertsen, Phys. Rev. B **41**, 10 058 (1990).
[45] R. G. Dandrea and A. Zunger, Phys. Rev. B **43**, 8962 (1991).
[46] S.-H. Wei and A. Zunger, J. Appl. Phys. **63**, 5794 (1988).
[47] D. B. Laks and A. Zunger, Phys. Rev. B **45**, 11 411 (1992).
[48] Note that experimentally the conduction-band minimum is found at the $\bar{M}(X_{x,y})$ point. However, as shown recently (Ref. 47), this is caused by interfacial interdiffusion; a truly abrupt monolayer superlattice has an L-type conduction-band minimum.
[49] Note that the experimental band gap is at the $\bar{M}(X_{x,y})$ point rather than at the calculated $\bar{\Gamma}(X_z)$ point. The reason is that in our calculation we assume that AlAs and GaAs are exactly lattice matched, whereas in fact they have a very small lattice mismatch of $\sim$0.1%. The resulting $X_{x,y} - X_z$ splitting pushes the in-plane state at $\bar{M}$ by about 20 meV below the perpendicular state at $\bar{\Gamma}$ (Ref. 42).
[50] The LRO η parameter is related to the fraction f of exchanged Ga and Al atoms in Ref. 47 by $\eta = 1 - 2f$.
[51] D. B. Laks, S.-H. Wei, and A. Zunger, Phys. Rev. Lett. **69**, 3766 (1992).
[52] A. Sasaki, J. Cryst. Growth **115**, 490 (1991).
[53] D. Leonard, M. Krishnamurthy, C. M. Reaves, S. P. Denbaars, and P. M. Petroff, Appl. Phys. Lett. **63**, 3203 (1993).
[54] A. Zrenner, L. V. Butov, M. Hagn, G. Abstreiter, G. Böhm, and G. Weimann, Phys. Rev. Lett. **72**, 3382 (1994).
[55] H. P. Hjalmarson, P. Vogl, D. J. Wolford, and J. D. Dow, Phys. Rev. Lett. **44**, 810 (1980).
[56] K. A. Mäder and A. Baldereschi, in *Advanced III-V Compound Semiconductor Growth, Processing and Devices*, edited by S. J. Pearton, D. K. Sadana, and J. M. Zavada, MRS Symposia Proceedings No. 240 (Materials Research Society, Pittsburgh, 1992), p. 597.
[57] L. Kleinman, Phys. Rev. B **21**, 2630 (1980).
[58] L. Kleinman and D. M. Bylander, Phys. Rev. Lett. **48**, 1425 (1982).
[59] D. E. Aspnes and A. A. Studna, Phys. Rev. B **7**, 4605 (1973).